Since January 2020 Elsevier has created a COVID-19 resource centre with free information in English and Mandarin on the novel coronavirus COVID-19. The COVID-19 resource centre is hosted on Elsevier Connect, the company's public news and information website.

Informatics in Medicine Unlocked 32 (2022) 101059

Contents lists available at ScienceDirect

Informatics in Medicine Unlocked

journal homepage: www.elsevier.com/locate/imu

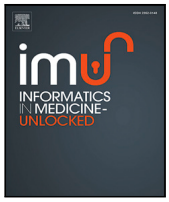

SEL-COVIDNET: An intelligent application for the diagnosis of COVID-19 from chest X-rays and CT-scans

Ahmad Al Smadi [a,b,*], Ahed Abugabah [b], Ahmad Mohammad Al-smadi [c], Sultan Almotairi [d,e]

[a] School of Artificial Intelligence, Xidian University, No. 2 South Taibai Road, Xian, 710071, China
[b] College of Technological Innovation, Zayed University, Abu Dhabi Campus, UAE
[c] Department of Computer Science, Al-Balqa Applied University, Ajloun University College, Jordan
[d] Faculty of Community College, Majmaah University, Al Majma'ah, Saudi Arabia
[e] Department of Information Systems, Faculty of Computer and Information Sciences, Islamic university of Madinah, 42351, Saudi Arabia

ARTICLE INFO

Keywords:
COVID-19
Transfer learning
X-ray images
CT-scans
Pneumonia
Deep Learning
Classification

ABSTRACT

COVID-19 detection from medical imaging is a difficult challenge that has piqued the interest of experts worldwide. Chest X-rays and computed tomography (CT) scanning are the essential imaging modalities for diagnosing COVID-19. All researchers focus their efforts on developing viable methods and rapid treatment procedures for this pandemic. Fast and accurate automated detection approaches have been devised to alleviate the need for medical professionals. Deep Learning (DL) technologies have successfully recognized COVID-19 situations. This paper proposes a developed set of nine deep learning models for diagnosing COVID-19 based on transfer learning and implementation in a novel architecture (SEL-COVIDNET). We include a global average pooling layer, flattening, and two dense layers that are fully connected. The model's effectiveness is evaluated using balanced and unbalanced COVID-19 radiography datasets. After that, our model's performance is analyzed using six evaluation measures: accuracy, sensitivity, specificity, precision, F1-score, and Matthew's correlation coefficient (MCC). Experiments demonstrated that the proposed SEL-COVIDNET with tuned DenseNet121, InceptionResNetV2, and MobileNetV3Large models outperformed the results of comparative SOTA for multi-class classification (COVID-19 vs. No-finding vs. Pneumonia) in terms of accuracy (98.52%), specificity (98.5%), sensitivity (98.5%), precision (98.7%), F1-score (98.7%), and MCC (97.5%). For the COVID-19 vs. No-finding classification, our method had an accuracy of 99.77%, a specificity of 99.85%, a sensitivity of 99.85%, a precision of 99.55%, an F1-score of 99.7%, and an MCC of 99.4%. The proposed model offers an accurate approach for detecting COVID-19 patients, which aids in the containment of the COVID-19 pandemic.

1. Introduction

The year 2020 was challenging for the entire planet and will be considered a year unlike any other. The world has seen the emergence of a unique coronavirus (COVID-19). The pandemic's effect extends beyond the loss of countless lives. It has far-reaching consequences for mental health, a perpetual state of terror, economic misery, and social disturbance, among other things. Worldwide, 594 million individuals have been infected, with over 6.5 million fatalities and 566 million recovery cases documented by August 08, 2022 [1]. Coronaviruses are a family of viruses that can cause illnesses such as the common cold, severe acute respiratory syndrome (SARS), and Middle East respiratory syndrome (MERS) [2]. Signs and symptoms of 2019-nCoV may appear 2 to 14 days after exposure. After exposure to the virus and before symptoms appear, this period is called the incubation period [3]. It can still spread the COVID-19 infection before developing symptoms. Common signs and symptoms may include fever, cough and tiredness, shortness of breath or difficulty breathing, etc. Symptoms of COVID-19 can range from very mild to severe. Some people have few symptoms [4]. COVID-19 therapy sometimes does not eradicate the virus; instead, it helps alleviate symptoms. Many approaches for detecting SARS-CoV-2 infection include real-time reverse transcription-polymerase chain reaction (RT-PCR), isothermal nucleic acid amplification, and microarrays [5]. Most nations' health authorities have adopted the RT-PCR technology, which is widely considered the standard for molecular diagnosis of viral and bacterial illnesses [6].

Doctors commonly use a reverse transcription-polymerase chain reaction (RT-PCR) test on blood and sputum specimens to diagnose COVID-19. This test detects evidence of the virus's biologically-derived

* Corresponding author at: School of Artificial Intelligence, Xidian University, No. 2 South Taibai Road, Xian, 710071, China.
E-mail address: ahmadsmadi16@yahoo.com (A.A. Smadi).

https://doi.org/10.1016/j.imu.2022.101059
Received 18 June 2022; Received in revised form 17 August 2022; Accepted 17 August 2022
Available online 24 August 2022

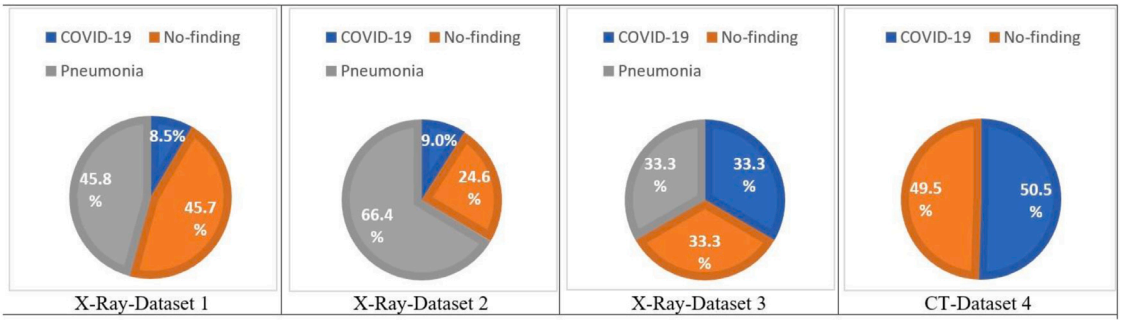

Fig. 1. Datasets distribution.

Table 1
A comparison of related work methods for detecting COVID-19 using CT scan images. (CAP) community-acquired pneumonia.

Study	Number of cases	Methods	Performance %
Wang et al. [7]	44 COVID-19 55 Viral Pneumonia	M-Inception	Accuracy of 73.1 for 2-classes
Zheng et al. [8]	313 COVID-19 229 No-findings	DeCovNet	Accuracy of 90.1 for 2-classes
Li et al. [9]	1296 COVID-19 1735 Pneumonia 1325 Non-Pneumonia	COVNet	Accuracy of 96 for 3-classes
Song et al. [10]	88 COVID-19 101 Bacteria Pneumonia 86 Healthy	DeepPneumonia	Accuracy of 94.0 for 2-classes Accuracy of 86.0 for 3-classes
Wang et al. [11]	325 COVID-19 740 Pneumonia	InceptionNet	Accuracy of 89.50 for 2-classes
Shi et al. [12]	1658 Non-COVID 1027 CAP	Random Forest	Accuracy of 87.9 for 2-classes
Li et al. [13]	1292 COVID-19 1735 CAP 1325 Non-Pneumonia	ResNet50 backbone	Accuracy of 96.3 for 3-classes
Xu et al. [14]	219 COVID-19 224 Influenza-A 175 Healthy	Attention oriented model based on ResNet18	Accuracy of 86.7 for 3-classes

Table 2
Hyperparameter configuration.

Parameters Activation Function	ReLU/Sigmoid/Sofmax
Base Learning Rate	0.001
Minimum Learning Rate	1e-5
Epochs	50
Batch Size	32
Optimizer	Adam
Loss Function	Binary Cross-Entropy for a binary classifier Categorical Cross-Entropy for multi-class classifier
Early Stopping patience	10
Monitor	Validation accuracy
Factor	0.1
ReduceLROnPlateau patience	2

component in the patient's blood. The virus's remnants do not start showing up effectively as a susceptible test. Numerous recent studies indicate that chest computer tomography (CT) works better than laboratory tests in screening for COVID-19 [15]. Chest computed tomography (CT) is a more accurate, effective, and rapid method of diagnosing COVID-19 than RT-PCR. Doctors commonly utilize chest CT imaging to diagnose pneumonia [16]. CT scans are used to provide comprehensive three-dimensional imaging of the lung. Doctors analyze chest CT scans for fluid or pus in the lungs or any other signs consistent with COVID-19 infection. Chest CTs are typically quick and painless to do [16].

Likewise, owing to the cheap cost and rapid image capture approach associated with chest radiograph (X-ray) image-based diagnostics, it may be a more appealing and accessible tool for identifying the beginning of the illness. Since technology has been used in medical research, medical equipment and diagnostics have advanced to a new level. In many different fields, including computer vision [17], healthcare systems [18], and most recently, COVID-19 diagnosis [19,20], deep-learning methods have been able to produce results that are considered to be state-of-the-art. This is owing to their capacity to autonomously extract representations from learning data that are important to their predictions. The state-of-the-art IoT gadgets have simplified difficult processes and aided in real-time monitoring—technology advances at a breakneck pace [21]. Today, researchers can produce a diversified and broad variety of substantial feature sets using deep learning, which is impossible for a professional to do [22]. Machine learning (ML) and deep learning (DL) have amassed a plethora of applications over the last several decades and have shown to be invaluable in resolving complex medical use cases [23]. For example, in order to comprehend how to tell a healthy lung from an infected lung, machine learning algorithms need to be organized and have a set of features to predict the outcome [24,25].

On the other hand, with DL, the classifier automatically identifies healthy lungs from infected lungs using network characteristics generated automatically [26]. With the ability to generate features autonomously, DL has developed into a strong tool that eliminates the need for human features extraction. DL algorithms have seen several

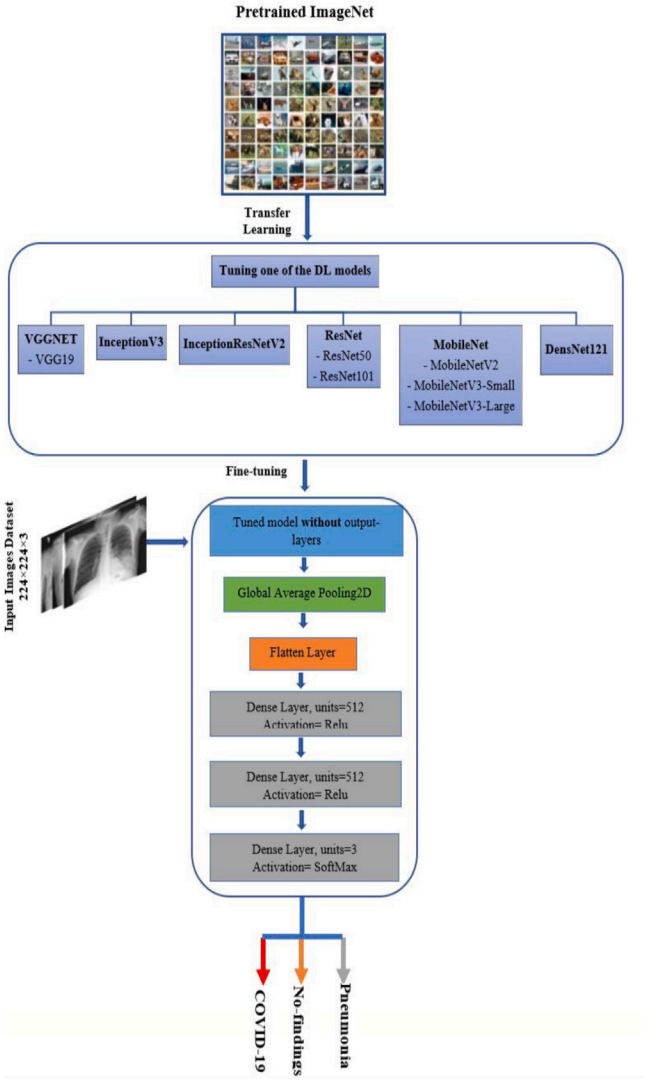

Fig. 2. Flowchart of proposed SEL-COVIDNET schematic for classifying the COVID-19 status in chest images.

advances over the decades and are now widely employed to identify problems in clinical imaging [27]. Therefore, deep learning algorithms can tackle new problems by using previously acquired information. When developing deep learning techniques with small datasets, areas of interest in those images are often incorrectly identified, a problem that is seldom covered in the current literature. As a result, we examined our models' performance and picked just the highest performing ones based on their ability to identify Covid-19 seen on X-ray images correctly.

Additionally, prior work often fails to illustrate how their suggested models function when confronted with unbalanced datasets, which is frequently problematic. We diversify our study in this section by considering small, unbalanced, and balanced and provide a full discussion of our findings. This article reviews current work on the subject and considers the possibility of presenting a successful deep learning-based screening technique for detecting patients with COVID-19 using chest X-ray and CT scan images and how our model overcomes earlier research's limitations. The literature's overwhelming studies fall into one of two classes (COVID-19 vs. No-finding). However, just a few articles addressed many classes. With expert-level automation, we anticipate that this technology will aid in the testing of COVID-19 patients. The following are the paper's significant contributions:

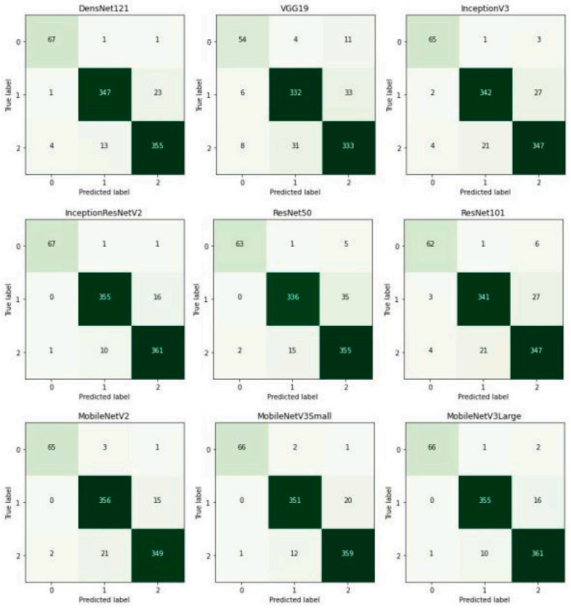

Fig. 3. Confusion matrix of multi-class DL models used in the SEL-COVIDNET on X-ray dataset 1. (0: COVID-19, 1: No-finding, 2: Pneumonia).

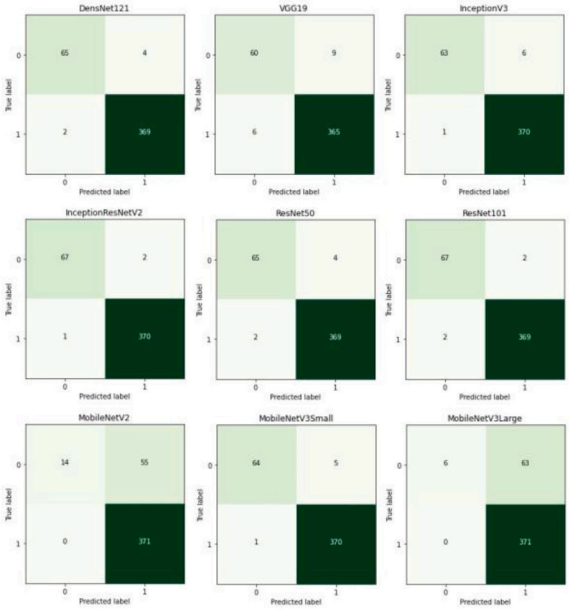

Fig. 4. Confusion matrix of binary-class DL models used in the SEL-COVIDNET on X-ray dataset 1. (0: COVID-19, 1: No-finding).

- This work developed a collection of deep learning models in a novel architecture (SEL-COVIDNET) to aid in the early identification of patients with COVID-19 efficiently.
- Comprehensive experiments were conducted on chest X-ray and CT scan images (Balanced dataset, Unbalanced dataset) to verify the proposed method's efficacy.
- Compared the proposed model to various state-of-the-art architectures in terms of deep feature extraction and categorization of COVID-19 chest X-ray and CT scan images.

Table 3
Evaluation performance of multi-class DL models used in the SEL-COVIDNET on X-ray dataset 1 (0: COVID-19, 1: No-finding, 2: Pneumonia). The best overall accuracy is reported in bold red.

Model	Class	Acc	Sen	Spc	Ppv	F1-Score	MCC	Overall Acc (%)
DensNet121	0	0.991	0.971	0.993	0.931	0.950	0.946	94.70
	1	0.953	0.935	0.968	0.961	0.948	0.906	
	2	0.950	0.954	0.945	0.937	0.945	0.899	
InceptionV3	0	0.988	0.942	0.992	0.915	0.929	0.922	92.86
	1	0.937	0.922	0.950	0.940	0.931	0.873	
	2	0.932	0.933	0.932	0.920	0.927	0.864	
VGG19	0	0.964	0.783	0.981	0.794	0.788	0.769	88.55
	1	0.909	0.895	0.921	0.905	0.900	0.816	
	2	0.898	0.895	0.900	0.883	0.889	0.794	
InceptionResNetV2	0	0.996	0.971	0.999	0.985	0.978	0.976	**96.43**
	1	0.967	0.957	0.975	0.970	0.963	0.933	
	2	0.966	0.970	0.961	0.955	0.963	0.931	
ResNet50	0	0.990	0.913	0.997	0.969	0.940	0.935	92.86
	1	0.937	0.906	0.964	0.955	0.929	0.874	
	2	0.930	0.954	0.909	0.899	0.926	0.861	
ResNet101	0	0.983	0.899	0.991	0.899	0.899	0.889	92.36
	1	0.936	0.919	0.950	0.939	0.929	0.871	
	2	0.929	0.933	0.925	0.913	0.923	0.857	
MobileNetV2	0	0.993	0.942	0.997	0.970	0.956	0.952	94.83
	1	0.952	0.960	0.946	0.937	0.948	0.904	
	2	0.952	0.938	0.964	0.956	0.947	0.903	
MobileNetV3Small	0	0.995	0.957	0.999	0.985	0.971	0.968	95.57
	1	0.958	0.946	0.968	0.962	0.954	0.916	
	2	0.958	0.965	0.952	0.945	0.955	0.916	
MobileNetV3Large	0	0.995	0.957	0.999	0.985	0.971	0.968	96.31
	1	0.967	0.957	0.975	0.970	0.963	0.933	
	2	0.964	0.970	0.959	0.953	0.961	0.928	

Table 4
Evaluation performance of binary-class DL models used in the SEL-COVIDNET on X-ray dataset 1 (0: COVID-19, 1: No-finding). The best overall accuracy is reported in bold red.

Model	Class	Acc	Sen	Spc	Ppv	F1-score	MCC	Overall Acc (%)
DensNet121	0	0.986	0.942	0.995	0.970	0.956	0.948	98.64
	1	0.986	0.995	0.942	0.989	0.992	0.948	
InceptionV3	0	0.984	0.913	0.997	0.984	0.947	0.939	98.41
	1	0.984	0.997	0.913	0.984	0.991	0.939	
VGG19	0	0.966	0.870	0.984	0.909	0.889	0.869	96.59
	1	0.966	0.984	0.870	0.976	0.980	0.869	
InceptionResNetV2	0	0.993	0.971	0.997	0.985	0.978	0.974	**99.32**
	1	0.993	0.997	0.971	0.995	0.996	0.974	
ResNet50	0	0.986	0.942	0.995	0.970	0.956	0.948	98.64
	1	0.986	0.995	0.942	0.989	0.992	0.948	
ResNet101	0	0.991	0.971	0.995	0.971	0.971	0.966	99.09
	1	0.991	0.995	0.971	0.995	0.995	0.966	
MobileNetV2	0	0.875	0.203	1.000	1.000	0.337	0.420	87.50
	1	0.875	1.000	0.203	0.871	0.931	0.420	
MobileNetV3Small	0	0.986	0.928	0.997	0.985	0.955	0.948	98.64
	1	0.986	0.997	0.928	0.987	0.992	0.948	
MobileNetV3Large	0	0.857	0.087	1.000	1.000	0.160	0.273	85.68
	1	0.857	1.000	0.087	0.855	0.922	0.273	

- Analyzed the proposed model's performance using six evaluation measures: sensitivity, specificity, precision, F1-score, accuracy, and Matthew's correlation coefficient (MCC). Thus, the proposed method outperforms relatively in comparison with SOTA methods.

The rest of this paper is organized as follows: The related work is detailed in Section 2. Material and methods are discussed in Section 2. The experimental results of the proposed SEL-COVIDNET are presented in Section 4. Comparative results and discussion are described in Section 5. Finally, the conclusion and future direction are presented in Section 6.

2. Related work

Deep learning has garnered much attention lately in the battle against the Covid-19 epidemic. Numerous deep learning algorithms have been recently presented as Covid-19 diagnostic tools to assist doctors in making more informed medical decisions. This section discusses much research that is relevant to this study.

Researchers have been concentrating their efforts on deep learning algorithms for identifying COVID-19 in chest X-rays. According to Das et al. [28], utilizing a DL-based network in lieu of CT scan scanners is a cost-effective option. Ozturk et al. [29] developed an architecture named DarkNet, a classifier model for classifying positive and negative COVID-19 chest X-ray images and a multi-class classifier for detecting

Table 5
Evaluation performance of multi-class DL models used in the SEL-COVIDNET on X-ray dataset 2 (0: COVID-19, 1: No-finding, 2: Pneumonia). The best overall accuracy is reported in bold red.

Model	Class	Acc	Sen	Spc	Ppv	F1-score	MCC	Overall Acc (%)
DensNet121	0	1.000	1.000	1.000	1.000	1.000	1.000	**98.52**
	1	0.985	0.965	0.992	0.975	0.970	0.960	
	2	0.985	0.991	0.975	0.987	0.989	0.967	
InceptionV3	0	0.998	1.000	0.997	0.975	0.987	0.986	97.75
	1	0.980	0.950	0.990	0.968	0.959	0.945	
	2	0.977	0.985	0.963	0.981	0.983	0.949	
VGG19	0	0.988	0.922	0.994	0.938	0.930	0.923	94.95
	1	0.956	0.912	0.970	0.909	0.910	0.881	
	2	0.956	0.967	0.933	0.966	0.967	0.901	
InceptionResNetV2	0	0.998	1.000	0.998	0.983	0.991	0.991	98.29
	1	0.984	0.959	0.993	0.977	0.968	0.958	
	2	0.983	0.989	0.970	0.985	0.987	0.962	
ResNet50	0	0.999	1.000	0.999	0.991	0.996	0.995	97.98
	1	0.981	0.950	0.991	0.971	0.960	0.947	
	2	0.980	0.988	0.963	0.981	0.985	0.955	
ResNet101	0	0.998	0.983	1.000	1.000	0.991	0.990	97.67
	1	0.978	0.953	0.987	0.959	0.956	0.941	
	2	0.977	0.985	0.961	0.980	0.982	0.948	
MobileNetV2	0	0.999	1.000	0.999	0.991	0.996	0.995	97.44
	1	0.975	0.927	0.991	0.970	0.948	0.932	
	2	0.973	0.988	0.941	0.974	0.981	0.938	
MobileNetV3Small	0	1.000	1.000	1.000	1.000	1.000	1.000	98.45
	1	0.984	0.962	0.992	0.974	0.968	0.958	
	2	0.984	0.991	0.972	0.986	0.988	0.965	
MobileNetV3Large	0	0.998	1.000	0.998	0.983	0.991	0.991	98.52
	1	0.986	0.959	0.995	0.984	0.971	0.962	
	2	0.986	0.993	0.972	0.986	0.990	0.969	

Table 6
Evaluation performance of binary-class DL models used in the SEL-COVIDNET on X-ray dataset 2 (0: COVID-19, 1: No-finding). The best overall accuracy is reported in bold red.

Model	Class	Acc	Sen	Spc	Ppv	F1-score	MCC	Overall Acc (%)
DensNet121	0	0.998	1.000	0.997	0.991	0.996	0.994	**99.77**
	1	0.998	0.997	1.000	1.000	0.998	0.994	
InceptionV3	0	0.998	1.000	0.997	0.991	0.996	0.994	99.77
	1	0.998	0.997	1.000	1.000	0.998	0.994	
VGG19	0	0.968	0.939	0.978	0.939	0.939	0.917	96.76
	1	0.968	0.978	0.939	0.978	0.978	0.917	
InceptionResNetV2	0	0.995	0.991	0.997	0.991	0.991	0.988	99.54
	1	0.995	0.997	0.991	0.997	0.997	0.988	
ResNet50	0	0.991	1.000	0.987	0.966	0.983	0.977	99.07
	1	0.991	0.987	1.000	1.000	0.994	0.977	
ResNet101	0	0.984	0.983	0.984	0.958	0.970	0.959	98.38
	1	0.984	0.984	0.983	0.994	0.989	0.959	
MobileNetV2	0	0.993	0.983	0.997	0.991	0.987	0.982	99.31
	1	0.993	0.997	0.983	0.994	0.995	0.982	
MobileNetV3Small	0	0.995	1.000	0.994	0.983	0.991	0.988	99.54
	1	0.995	0.994	1.000	1.000	0.997	0.988	
MobileNetV3Large	0	0.993	1.000	0.991	0.975	0.987	0.983	99.31
	1	0.993	0.991	1.000	1.000	0.995	0.983	

COVID-19, pneumonia, and normal images. Khan et al. [30] utilized the ImageNet dataset for training the Xception model as a pre-trained network. Apostolopoulos et al. [31] trained a model from scratch and retrieved features for the classification task using MobileNet. Ucar et al. [32] employed the Bayesian optimization approach to optimize the SqueezeNet model on the COVID-19 diagnostic.

Loey et al. [33] constructed the model using generative adversarial networks (GANs) and transfer learning with multi-class classifiers for detecting COVID-19, pneumonia, and normal images. Luz et al. [34] improved the EfficientNet model to classify COVID-19 using chest X-ray images.

Chhikara et al. [35] built a deep transfer learning-based model using Inception-V3-Net to detect COVID-19 from chest X-rays and CT scans. Apostolopoulos et al. [36] introduced a deep learning-based diagnostic method for COVID-19. A binary classifier model and a multi-class classifier were conducted for COVID-19 detection. Hemdan et al. [37] developed a COVIDX-Net model for COVID-19 detection using seven distinct deep models. Mehmood et al. [38] proposed a DL-based technique using batch normalization for classifying three binary classes. Abugabah et al. [39] proposed a COVID-3D-SCNN model and attained promising results for multi-classification of COVID-19.

As a result, many researchers have proposed deep learning methods for detecting COVID-19 based on X-ray images [38,40–47]. More information about other work methods for detecting COVID-19 using X-ray images is depicted in Table 11 (see in Appendix).

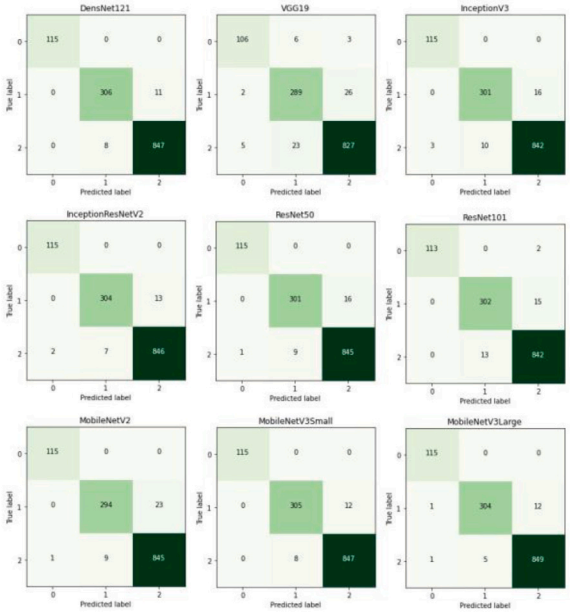

Fig. 5. Confusion matrix of multi-class DL models used in the SEL-COVIDNET on X-ray dataset 2. (0: COVID-19, 1: No-finding, 2: pneumonia).

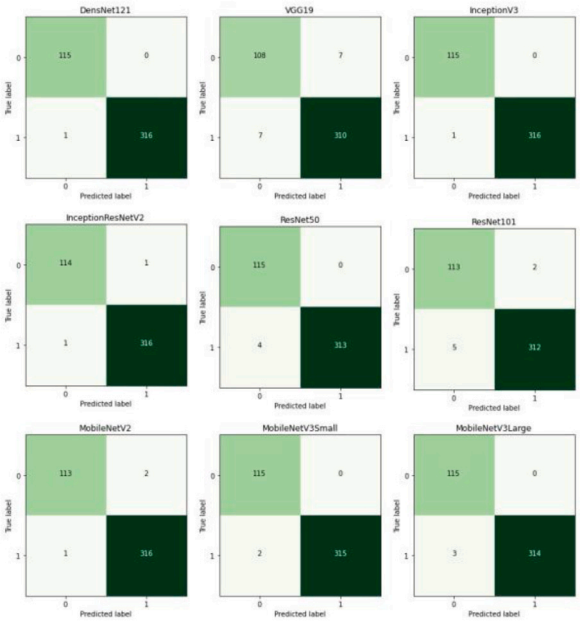

Fig. 6. Confusion matrix of binary-class DL models used in the SEL-COVIDNET on X-ray dataset 2. (0: COVID-19, 1: No-finding).

Additionally, other studies have indicated deep learning algorithms for COVID-19 detection based on CT scans. Wang et al. [7] developed the M-Inception model for classifying viral pneumonia and COVID-19. Their method attained a total accuracy of the test dataset of 73.1%. Zheng et al. [8] introduced a novel deep learning model (DeCovNet) that achieved a 90.1% accuracy rate. Li et al. [9] presented the COVNet model trained using ResNet50. The experimental findings indicated that the COVNet model had an accuracy of 0.96 for the COVID-19 classification. Song et al. [10] created a deep learning model (DeepP-neumonia) for COVID-19 detection. The model's overall accuracy for

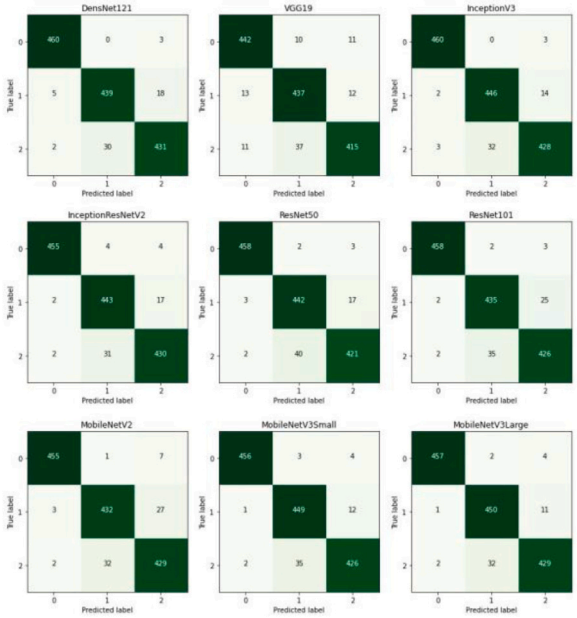

Fig. 7. Confusion matrix of multi-class DL models used in the SEL-COVIDNET on X-ray dataset 3. (0: COVID-19, 1: No-finding, 2: Pneumonia).

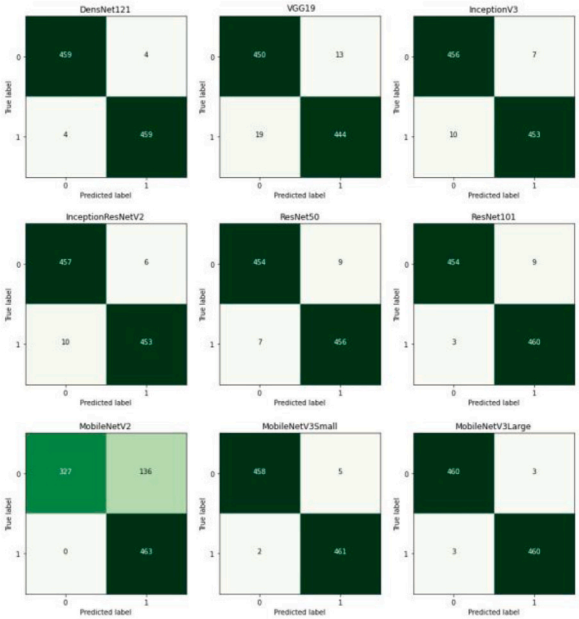

Fig. 8. Confusion matrix of binary-class DL models used in the SEL-COVIDNET on X-ray dataset 3. (0: COVID-19, 1: No-finding). The best overall accuracy is reported in bold red.

COVID-19 vs. bacterial pneumonia classification was 86.0%, while its overall accuracy for COVID-19 vs. healthy person classification was 94.0%. Table 1 has more information about other work methods for detecting COVID-19 with CT scans.

3. Material and methods

This section describes datasets and the pre-trained CNNs utilized to complete the proposed SEL-COVIDNet architecture.

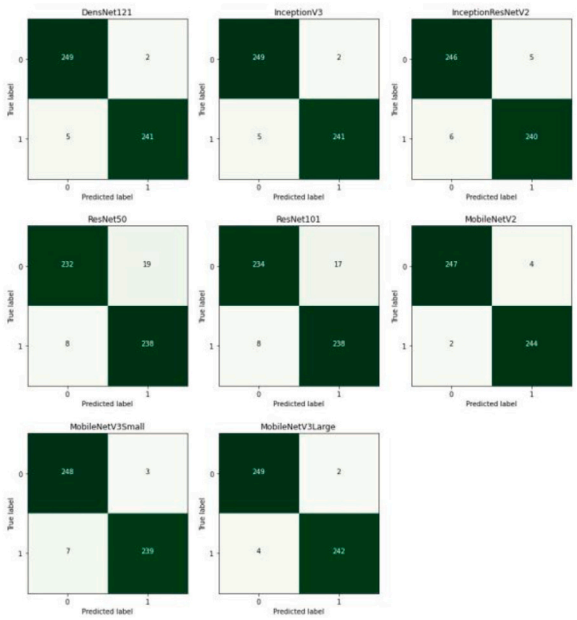

Fig. 9. Confusion matrix of DL models used in the SEL-COVIDNET on CT dataset 4. (0: COVID-19, 1: No-finding).

3.1. Dataset description

COVID-19 infection cases have now surpassed 457 million worldwide, with an estimated 6 million deaths [1]. However, severely contaminated nations have attempted to openly share clinical and radiographic data. Thereby, we have used three publicly available datasets, including as follows:

(a) X-ray-Dataset 1: We collected this data from two different sources; source one is named "X-ray Image DataSet [48]" with 125 COVID-19, 500 no-findings, and 500 pneumonia. The second source was obtained by a team of researchers from different universities [49]. It is worth mentioning that the first release of this source was used, which has 219 COVID-19 positive images, 1341 no-findings, and 1345 pneumonia images. To sum up, dataset 1 consists of three classes, including COVID-19, No-finding, and pneumonia. The total number of images is 344, 1841, and 1845, respectively.
(b) X-ray-Dataset 2: Unbalanced data divided into three classes [50]. The total number of images for the COVID-19, No-findings, and pneumonia classes is 576, 1583, and 4273.
(c) X-ray-Dataset 3: Balanced data is divided into three classes [51]. 6939 samples were collected, with 2313 samples being utilized in each category.
(d) CT-Dataset 4: This dataset, named the "SARS-CoV-2" CT scan dataset, has 1252 CT scans of patients tested positive for (COVID-19) and 1229 CT scans of patients who tested negative for COVID-19, totaling 2481 CT scans. These statistics were gathered from genuine patients in Sao Paulo, Brazil-hospitals [52].

Fig. 1 illustrates the distribution of the used datasets.

3.2. Pre-trained CNNs

(a) **VGGNet**:
VGGNet was developed by Karen Simonyan and Andrew Zisserman based on the CNN architecture [53]. The VGGNet functioned magnificently on the imageNet dataset. To increase image extraction capabilities, the VGGNet employed smaller filters of 3×3, as opposed to the AlexNet filter of 11×11. VGG16 and VGG19 are two variants of this deep network design with varying depths and layers. VGG19 is a deeper version of VGG16. However, the amount of parameters in VGG19 is greater, making it more costly to train the network than in VGG16.
(b) **InceptionV3:**
Inception v3 is an improved version of the Inception family's CNN design, and it was introduced by Szegedy et al. [54], which is the third version of Google's Inception CNN. Inceptionv3 was designed to allow for deeper networks while limiting the number of parameters to "around 25 million" compared to 60 million for AlexNet [55].
(c) **InceptionResNetV2:**
InceptionResNet-V2 derives from the Inception V3 model, and it is far deeper than the InceptionV3. It has 164 layers and is composed of Inception and residual connections. InceptionResNet-V2 is trained on images from the ImageNet collection totaling over a million [56].
(d) **Residual Network (ResNet):**
ResNet was first developed in 2015 by Kaiming He et al. [57] at Microsoft. ResNet's central concept is to provide an "identity shortcut connection" that bypasses one or more layers. ResNet comes in various variations that all operate on the same principle but have various layers, such as ResNet-34, ResNet-50, and ResNet-101.
(e) **MobileNetV2:**
MobileNetV2 was first developed by Sandler et al. [58]. It is optimized for systems with limited processing capacity. It is built on an inverted residual structure, with residual connections between bottleneck layers.
(f) **MobileNetV3:**
MobileNetV3 is a new generation of MobileNetV2 that was first developed by Howard et al. [59]. It has been tailored to mobile phone Processors using a combination of hardware-aware network architecture search (NAS) and the NetAdapt algorithm and then enhanced further using innovative architectural advancements. MobileNetV3 comes in two terminologies that operate on the same principle, MobileNetV3-Large, and MobileNetV3-Small. Compared to MobileNetV2, the authors in [59] stated that the MobileNetV3-Large is 3.2% more accurate in ImageNet classification while reducing latency by 15%. MobileNetV3-Small is 4.6% more accurate than MobileNetV2 while lowering latency by 5%.
(g) **DenseNet:**
DenseNet was first developed in 2016 by Huang et al. [60]. It solves the vanishing gradient problem, makes feature propagation stronger, encourages feature reuse, and significantly reduces the number of parameters.

3.3. Proposed SEL-COVIDNET description

We developed a novel classification model for determining the COVID-19 status in 2D chest images. Fig. 2 displays the whole process of our proposed SEL-COVIDNET, which is built on nine distinct DL architectures: DenseNet121, VGG19, InceptionV3, InceptionResNetV2, ResNet50, ResNet101, MobileNetV2, MobileNetV3-Small, and MobileNetV3-Large.

The SEL-COVIDNET framework consists of several steps that enable the classification of novel COVID19. Firstly, starting with preprocessing, all chest images are collected in a single dataset and scaled to a fixed size of 224×224 pixels. The preprocessed dataset is divided 80–20 to begin the training phase of one of nine deep learning models that have been tuned. Thereby, 20% of images will be exploited during the testing stage. It is worth mentioning that we use the pre-trained ImageNet weights for the tuned model.

Table 7
Evaluation performance of multi-class DL models used in the SEL-COVIDNET on X-ray dataset 3-Balanced (0: COVID-19, 1: No-finding, 2: Pneumonia). The best overall accuracy is reported in bold red.

Model	Class	Acc	Sen	Spc	Ppv	F1-score	MCC	Overall Acc (%)
DensNet121	0	0.993	0.994	0.992	0.985	0.989	0.984	95.82
	1	0.962	0.950	0.968	0.936	0.943	0.914	
	2	0.962	0.931	0.977	0.954	0.942	0.914	
InceptionV3	0	0.994	0.994	0.995	0.989	0.991	0.987	96.11
	1	0.965	0.965	0.965	0.933	0.949	0.923	
	2	0.963	0.924	0.982	0.962	0.943	0.915	
VGG19	0	0.968	0.955	0.974	0.948	0.952	0.927	93.23
	1	0.948	0.946	0.949	0.903	0.924	0.885	
	2	0.949	0.896	0.975	0.947	0.921	0.884	
InceptionResNetV2	0	0.991	0.983	0.996	0.991	0.987	0.981	95.68
	1	0.961	0.959	0.962	0.927	0.943	0.913	
	2	0.961	0.929	0.977	0.953	0.941	0.912	
ResNet50	0	0.993	0.989	0.995	0.989	0.989	0.984	95.17
	1	0.955	0.957	0.955	0.913	0.934	0.901	
	2	0.955	0.909	0.978	0.955	0.931	0.899	
ResNet101	0	0.994	0.989	0.996	0.991	0.990	0.985	95.03
	1	0.954	0.942	0.960	0.922	0.931	0.897	
	2	0.953	0.920	0.970	0.938	0.929	0.894	
MobileNetV2	0	0.991	0.983	0.995	0.989	0.986	0.979	94.81
	1	0.955	0.935	0.964	0.929	0.932	0.898	
	2	0.951	0.927	0.963	0.927	0.927	0.890	
MobileNetV3Small	0	0.993	0.985	0.997	0.993	0.989	0.984	95.89
	1	0.963	0.972	0.959	0.922	0.946	0.919	
	2	0.962	0.920	0.983	0.964	0.941	0.914	
MobileNetV3Large	0	0.994	0.987	0.997	0.993	0.990	0.985	**96.25**
	1	0.967	0.974	0.963	0.930	0.951	0.927	
	2	0.965	0.927	0.984	0.966	0.946	0.920	

Table 8
Evaluation performance of binary-class DL models used in the SEL-COVIDNET on X-ray dataset 3-Balanced (0: COVID-19, 1: No-finding). The best overall accuracy is reported in bold red.

Model	Class	Acc	Sen	Spc	Ppv	F1-score	MCC	Overall Acc (%)
DensNet121	0	0.991	0.991	0.991	0.991	0.991	0.983	99.14
	1	0.991	0.991	0.991	0.991	0.991	0.983	
InceptionV3	0	0.982	0.985	0.978	0.979	0.982	0.963	98.16
	1	0.982	0.978	0.985	0.985	0.982	0.963	
VGG19	0	0.965	0.972	0.959	0.959	0.966	0.931	96.54
	1	0.965	0.965	0.972	0.972	0.965	0.931	
InceptionResNetV2	0	0.983	0.987	0.978	0.979	0.983	0.965	98.27
	1	0.983	0.978	0.987	0.987	0.983	0.965	
ResNet50	0	0.983	0.981	0.985	0.985	0.983	0.965	98.27
	1	0.983	0.985	0.981	0.981	0.983	0.965	
ResNet101	0	0.987	0.981	0.994	0.993	0.987	0.974	98.70
	1	0.987	0.994	0.981	0.981	0.987	0.974	
MobileNetV2	0	0.853	0.706	1.000	1.000	0.828	0.739	85.31
	1	0.853	1.000	0.706	0.773	0.872	0.739	
MobileNetV3Small	0	0.992	0.989	0.996	0.996	0.992	0.985	99.24
	1	0.992	0.996	0.989	0.989	0.992	0.985	
MobileNetV3Large	0	0.994	0.994	0.994	0.994	0.994	0.987	**99.35**
	1	0.994	0.994	0.994	0.994	0.994	0.987	

The output of the tuned pre-trained model is used without the top output layers; after that, it runs through the Global Average Pooling (GAP) layer. GAP has some advantages, like making sure that feature maps and categories match up. Another benefit of global average pooling is that there is no parameter to optimize, so over-fitting is not a problem at this layer, i.e., GAP sums up the spatial information, so it is more resistant to changes in the input that move the data around [68]. Then, the output layer is flattened in order to stack two fully connected dense layers with nodes of 512 and 512, respectively. The dense layer provides learned features derived from the preceding layer's combinational features. These two fully connected dense layers contain 'ReLU' as an activation function. Hence, the number of classes to be predicted is two for the binary classifier model and three for a multi-class classifier. Therefore, we add a final output fully connected layer having two/three nodes using 'Sigmoid' as an activation function for the binary classifier and 'Softmax' as an activation function for the multi-class classifier.

The SEL-COVIDNET model is based on DL, which uses different hyperparameters for training. We used the categorical cross-entropy loss function and Adam optimizer as an optimization algorithm for controlling sparse gradients on noisy issues for a multi-class classifier. While a binary cross-entropy for a binary-class classifier.

4. Experiments and analysis

The SEL-COVIDNET framework, including deep learning models, has been implemented using Python in the Google Colab notebook

Table 9
Evaluation performance of binary-class DL models used in the SEL-COVIDNET on CT dataset 4 (0: COVID-19, 1: No-finding). The best overall accuracy is reported in bold red.

Model	Class	Acc	Sen	Spc	Ppv	F1-score	MCC	Overall Acc (%)
DensNet121	0	0.992	0.996	0.989	0.989	0.992	0.984	98.59
	1	0.992	0.989	0.995	0.996	0.992	0.984	
InceptionV3	0	0.986	0.992	0.980	0.980	0.986	0.972	98.59
	1	0.986	0.980	0.992	0.992	0.986	0.972	
InceptionResNetV2	0	0.978	0.980	0.976	0.976	0.978	0.956	97.79
	1	0.978	0.976	0.980	0.980	0.978	0.956	
ResNet50	0	0.946	0.924	0.967	0.967	0.945	0.892	94.57
	1	0.946	0.967	0.924	0.926	0.946	0.892	
ResNet101	0	0.950	0.932	0.967	0.967	0.949	0.900	94.97
	1	0.950	0.967	0.932	0.933	0.950	0.900	
MobileNetV2	0	0.988	0.984	0.992	0.992	0.988	0.976	98.79
	1	0.988	0.992	0.984	0.984	0.988	0.976	
MobileNetV3Small	0	0.980	0.988	0.972	0.973	0.980	0.960	97.99
	1	0.980	0.972	0.988	0.988	0.980	0.960	
MobileNetV3Large	0	0.988	0.992	0.984	0.984	0.988	0.976	**98.79**
	1	0.988	0.984	0.992	0.992	0.988	0.976	

Table 10
Comparison between the SEL-COVIDNET model and SOTA methods. CAP denotes community-acquired pneumonia.

Model	Dataset Type	Overall Acc (%)	Ppv (%)	Ses (%)	F1-Score (%)
Wang et al. [11]	X-ray (Normal vs. COVID-19 vs. Pneumonia)	93.3	90.9%	96.8%	N/A
Wang et al. [7]	CT Scans (COVID-19 vs. Non-COVID-19)	89.5	N/A	0.87	N/A
Al-Falluji et al. [61]	X-ray (Normal vs. COVID-19 vs. Pneumonia)	96.37	100%	94%	N/A
Singh et al. [62]	X-ray (Normal vs. COVID-19 vs. Pneumonia)	95.8	96.16	95.60	95.88
Abbas et al. [63]	X-ray (Normal vs. COVID-19 vs. SARS)	95.12	N/A	97.91	N/A
Ozturk et al. [29]	X-ray (Normal vs. COVID-19 vs. Pneumonia)	87.02	N/A	N/A	N/A
Luz et al. [34]	X-ray (Normal vs. COVID-19 vs. Pneumonia)	93.51	100.0%	80.6%	N/A
Montalbo [64]	X-ray (Normal vs. COVID-19 vs. Pneumonia)	97.99	98.38	98.15	98.26
Abugabah et al. [39]	X-ray (Normal vs. COVID-19 vs. Pneumonia)	96.70	N/A	96.62	N/A
Shi et al. [12]	CT (COVID-19 vs. CAP)	87.9	N/A	90.70	N/A
Qjidaa et al. [65]	X-ray (Normal vs. COVID-19 vs. Pneumonia)	98	98.66	98.33	98.30
Chhikara et al. [35]	X-ray and CT scans (Normal vs. COVID-19 vs. Pneumonia)	97.70	97.6	97.6	97.6
Montalbo [66]	X-ray and CT scans (Normal vs. COVID-19 vs. Pneumonia)	97.41	97.59	97.52	97.55
Saad et al. [67]	X-ray and CT scans (COVID-19 vs. Non-Covid)	99.3	99.79	98.8	99.3
Li et al. [13]	CT Scans (COVID-19 vs. CAP vs. Non-Pneumonia)	96.3	N/A	90	N/A
Xu et al. [14]	CT Scans (COVID-19 vs. Influenza-A vs. Healthy)	86.7	86.9	86.7	86.7
Proposed SEL-COVIDNET (Tuned DenseNet121)	X-ray and CT scans (COVID-19 vs. No-finding vs. Pneumonia)	98.52	98.7	98.5	98.6

using the graphical processing unit (GPU). It is worth mentioning that all the models are trained for 50 epochs. As a result, this study used a callback function called Reduce LR on Plateau (RLRoP) to improve the models' grasp and flexibility throughout training without putting a significant demand on computer resources [69]. We employed the early stopping that the model can stop training once the validation error reaches the minimum. Table 2 shows the hyperparameters for the proposed method.

We employed six different metrics to examine the accuracy of COVID-19 categorization in the testing chest images to determine the efficacy of each DL model in the SEL-COVIDNET. The accuracy (Acc), sensitivity (Sen), specificity (Spc), positive predictive value-precision (Ppv), F1-score, and Matthew's correlation coefficient (MCC) quantify the actual and predicted classes represented in Eq. (1)- 6, respectively. Mathematically, each performance statistic is denoted as follows:

$$Acc = \frac{TP + TN}{TP + FP + FN + TN} \quad (1)$$

Table 11
An overview comparison of related work methods for detection of COVID-19 using chest X-ray images.

Study	Number of cases	Methods	Performance
Ozturk et al. [29]	125 with COVID-19 500 normal 500 pneumonia	DarkCovidNet	Accuracy of 87.02 for 3-classes Accuracy of 98.08 2-class
Khan et al. [30]	290 COVID-19 1203 Normal 931 Viral Pneumonia 660 Bacterial Pneumonia	CoroNet	Accuracy of 95 for 3-classes Accuracy of 89.6 for 4-classes
Apostolopoulos et al. [31]	A large-scale dataset of 3905 7-classes	MobileNet v2	Accuracy of 87.66 for 7-classes Accuracy of 99.18 for 2-classes
Loey et al. [33]	69 COVID-19 79 Normal 79 Bacterial Pneumonia 79 Pneumonia	GAN transfer learning models (Alexnet, Googlenet, Resnet18)	Accuracy of 80.56 for 4-classes Accuracy of 85.19 for 3-classes Accuracy of 100 for 2-classes
Luz et al. [34]	152 COVID-19 7966 Normal 5421 Pneumonia	EfficientNe	Accuracy of 93.9 for 3-classes
Chhikara et al. [35]	2313 COVID-19 2313 Normal, 2313 Viral Pneumonia	Inception-V3	Accuracy of 84.95 for 3-classes
Apostolopoulos et al. [36]	224 COVID-19 700 Bacterial Pneumonia 504 Normal	VGG19	Accuracy of 98.75 for 2-classes Accuracy of 93.48 for 3-classes
Hemdan et al. [37]	25 COVID-19 25 Non-covid	COVIDX-Net	Accuracy of 90 for 2-classes
Maia et al. [40]	217 COVID-19 108 Other Diseases 112 Healthy	Convolutional SVM	Accuracy of 98.14 for 3-classes
Ibrahim et al. [41]	371 COVID-19 4237 Non-COVID-19 4078 Bacterial Pneumonia 2882 Healthy	AlexNet	Accuracy of 99.62 for 2-classes Accuracy of 94.00 for 3-classes Accuracy of 93.42 for 4-classes
Sethy et al. [42]	25 COVID-19 25 Non-Covid	ResNet50+SVM	Accuracy of 95.38 for 2-classes
Suat et al. [43]	331 COVID-19 1050 Pneumonia 1050 Non-Covid	CapsNet	Accuracy of 97.24 for 2-classes Accuracy of 84.22 for 3-classes
Zhang et al. [44]	70 COVID-19 1008 Pneumonia	CNN+Backbone network	Accuracy of 95.2 for 2-classes
Ghoshal et al. [45]	68 COVID-19 2786 Bacterial Pneumonia 1583 Normal 1504 Viral Pneumonia	Bayesian CNN+Dropweights	Accuracy of 92.90 for 4-classes
Panwar et al. [46]	142 COVID-19 142 Normal	nCOVnet	Accuracy of 88 for 2-classes
Rahman et al. [47]	3616 COVID-19 8851 Normal 6012 Non-COVID	DenseNet201	Accuracy of 95.11 for 3-classes
Mehmood et al. [38]	1290 COVID-19 1946 Normal	CNN-based technique using batch normalization	Accuracy of 96.6 for 2-classes
Montalbo [64]	1281 COVID-19 3270 Normal 4657 Pneumonia	Truncated DenseNet	Accuracy of 97.8 for 3-classes
Abugabah et al. [39]	575 COVID-19 1200 Non-COVID 1400 Pneumonia	COVID-3D-SCNN	Accuracy of 96.7 for 3-classes
Saad et al. [67]	2628 COVID-19 1620 Non-COVID	Deep feature concatenation technique (DFC)	Accuracy of 99.3 for 2-classes

$$Sen = \frac{TP}{TP + FN} \tag{2}$$

$$Spc = \frac{TN}{TN + FP} \tag{3}$$

$$Ppv = \frac{TP}{TP + FP} \tag{4}$$

$$F1 - score = 2 \times \frac{Ppv \times Sen}{Ppv + Sen} \tag{5}$$

$$\text{MCC} = \frac{TP \times TN - FP \times FN}{\sqrt{(TP + FP)(TP + FN)(TN + FP)(TN + FN)}} \tag{6}$$

Where "TP", "TN", "FP", "FN" stand for true positive, true negative, false positive, and false negative, respectively.

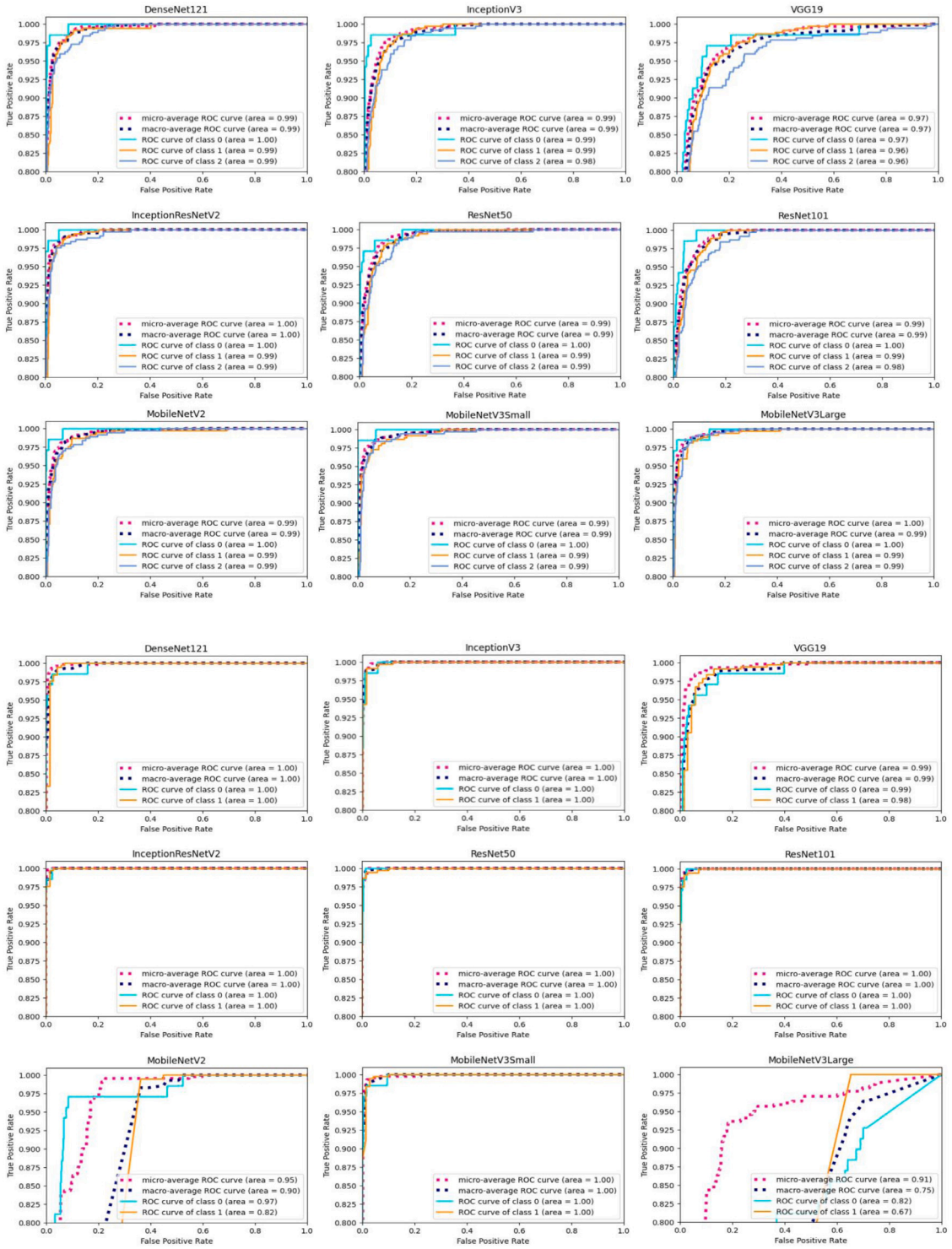

Fig. 10. Receiver operating characteristic of DL models used in the SEL-COVIDNET on X-ray dataset 1. The top side illustrates the 3-class classification, and the bottom side shows the 2-class classification.

4.1. Performance evaluation on X-ray-Dataset 1

Among all 3-class DL models used in the SEL-COVIDNET, the VGG19 model had the lowest accuracy of 88.55%, while the InceptionResNetV2 and MobileNetV3Large models had the highest accuracy scores, 96.43% and 96.31%, respectively. Regarding individual class accuracy, the InceptionResNetV2 had an accuracy of 99.6% for the COVID-19 class, followed by MobileNetV3Small. Both MobileNetV3Small and MobileNetV3Large had nearly identical accuracy for the other two classes. Table 3 depicts a detailed comparison of multi-class DL models using X-ray-Dataset 1. Moreover, for the binary-class DL models used in the SEL-COVIDNET, the MobileNetV2 model had the lowest accuracy of 87.5%. In contrast, the InceptionResNetV2 model had the highest accuracy scores, 99.32%, followed by the ResNet101 model. Similarly, the same model had the best accuracy of 99.3% for the COVID-19 class for individual class accuracy. Table 4 depicts a detailed comparison of binary-class DL models using X-ray-Dataset 1. The confusion matrix

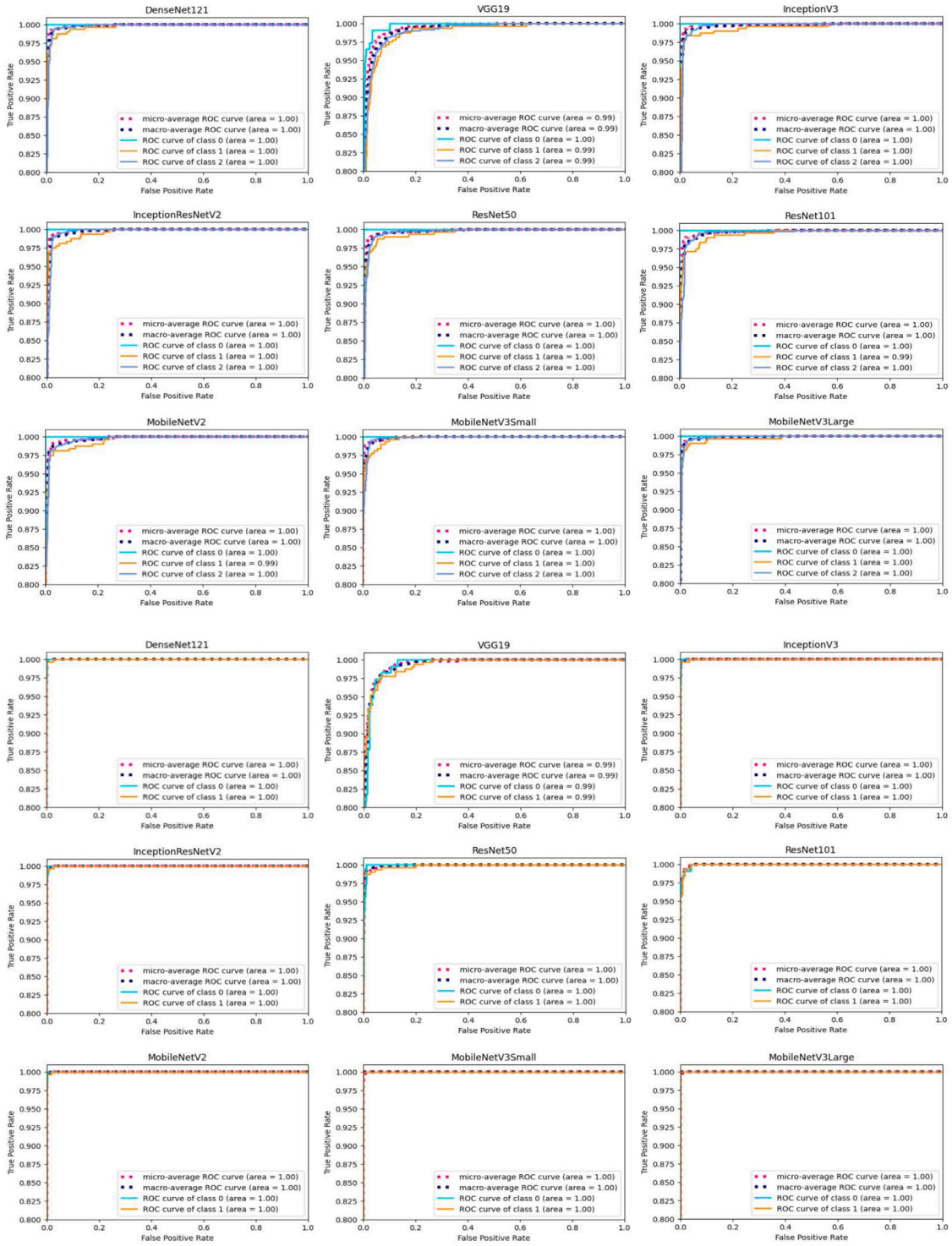

Fig. 11. Receiver operating characteristic of DL models used in the SEL-COVIDNET on X-ray dataset 2. The top side illustrates the 3-class classification, and the bottom side shows the 2-class classification.

of the DL models used in the SEL-COVIDNET on the test X-ray-Dataset 1 is shown in Figs. 3 and 4.

4.2. Performance evaluation on X-ray-Dataset 2

Here, all models showed an overall accuracy of above 94%. And out of these models, both DensNet121 and MobileNetV3Large outperformed the rest of the models with an overall accuracy of 98.52%. Regarding COVID-19 class accuracy, the DenseNet121 and MobileNetV3Small models performed well. All models showed an overall accuracy of above 98% for the binary class. And out of these models, both DensNet121 and InceptionV3 outperformed the rest of the models with an overall accuracy of 99.77%. Tables 5–6 depict a detailed comparison of multi-class and binary-class DL models using X-ray-Dataset 2. The confusion matrix of the DL models used in the SEL-COVIDNET on the test X-ray-Dataset 2 is shown in Figs. 5 and 6

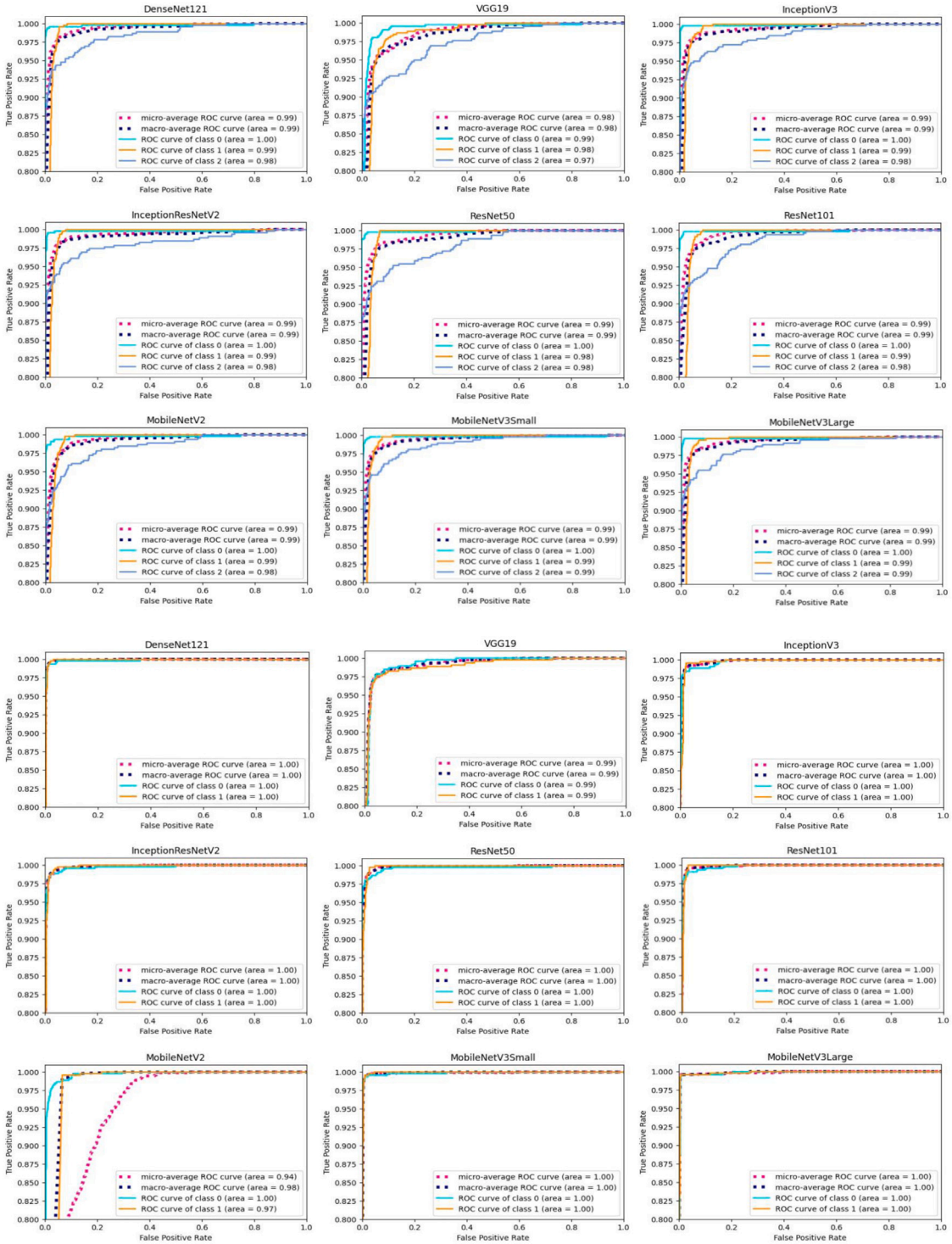

Fig. 12. Receiver operating characteristic of DL models used in the SEL-COVIDNET on X-ray dataset 3. The top side illustrates the 3-class classification, and the bottom side shows the 2-class classification.

4.3. Performance evaluation on X-ray-Dataset 3

On the balanced X-ray-Dataset 3, all models showed an overall accuracy of above 93%. And out of these models, the MobileNetV3Large outperformed the rest of the models with an overall accuracy of 96.25%. For the individual class accuracy, the same model performed well. Concerning binary-class classification on the same dataset, all models showed an overall accuracy of above 96%, except the MobileNetV2 model attained an accuracy of 85.31%. Tables 7–8 compare multi-class and binary-class DL models using X-ray-Dataset 3. The confusion matrix of the DL models used in the SEL-COVIDNET on the test X-ray-Dataset 3 is shown in Figs. 7 and 8

4.4. Performance evaluation on CT-Dataset 4

Out of the DL models used in the SEL-COVIDNET on the test CT-Dataset, both MobileNetV3Large and MobileNetV2 models outperformed the rest with an overall accuracy of 98.79%, followed by

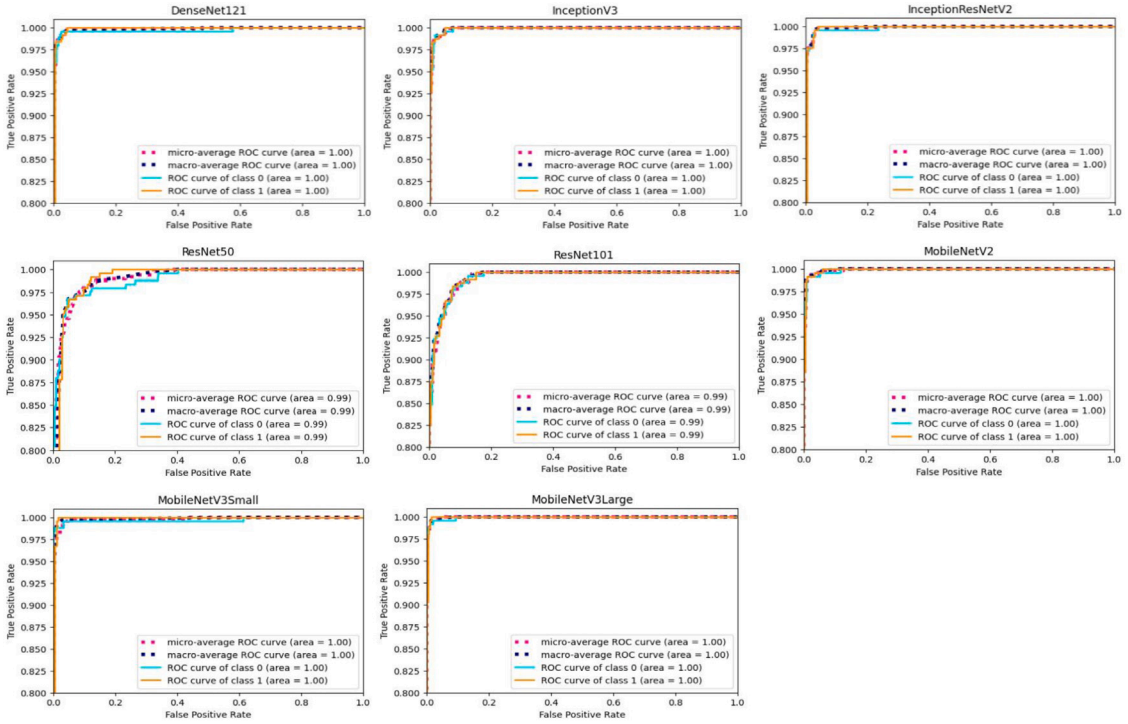

Fig. 13. Receiver operating characteristic of DL models used in the SEL-COVIDNET on CT dataset 4.

DensNet121 with an overall accuracy of 98.55%. It is worth mentioning that the VGGNET has been omitted for this experiment due to its bad performance. Table 9 depicts a detailed comparison of DL models using CT-Dataset. The confusion matrix of the DL models used in the SEL-COVIDNET on the test CT-Dataset is shown in Fig. 9.

4.4.1. Analysis of the DL models' receiver operating characteristic (ROC) curves on the used datasets:

ROC is a critical assessment statistic for determining the success of any classification model. Besides, the area under the curve (AUC) represents the degree or measure of separability. It indicates the capability of the model for discriminating between classes. The larger the AUC, the more accurately the model predicts. This subsection analyzes the AUC-ROC for used DL models in the SEL-COVIDNET for the conducted dataset.

Fig. 10 (see in Appendix). shows the AUC-ROC for used DL models in the SEL-COVIDNET on X-ray dataset 1. It can be observed from the left side of this figure that all of the models achieved amazing performances across all of their respective classes. Despite this, the VGG19 model had attained the lowest macro average of 0.97 and had noisy oscillations on its graph. Similarly, for binary class classification on the right side of the exact figure, the MobileNetV2 and MobileNetV3Large models had noisy oscillations on their graphs. In particular, DenseNet121, InceptionV3, InceptionResNetV2, RenNet, and MobileNetV3Small models achieved AUROCs of 1.00 across all regions, indicating that they outperformed the other DL models.

The AUC-ROC for X-ray dataset 2 is shown in Fig. 11 (see in Appendix). We can observe that all of the models attained remarkable results across their respective classes. In 2-class classification (COVID-19 vs. No-finding), all models except the VGG19 model had AUROCs of 1.00 in all regions except for the VGG19 model.

Regarding X-ray dataset 3, Its AUC-ROC figure is shown in Fig. 12 (see in Appendix). The lowest macro-average of 0.98 was attained by the VGG19 model for 3-class classification (COVID-19 vs. No-finding vs. pneumonia) and the MobileNetV2 model for 2-class classification (COVID-19 vs. No-finding). As noted, the model derives its lowest AUROC of 0.97 from X-ray images of patients infected with pneumonia at lower thresholds. The truncation's unfavorable impacts were also seen in most graphs of the DL models concerning pneumonia class.

The AUC-ROC graph on CT scan dataset 4 is depicted in Fig. 13 (see in Appendix). It can be observed that DenseNet121, InceptionV3, InceptionResNetV2, MobileNetV2, and MobileNetV3 all had AUROCs of 1.00 across all regions, which means they did better than the other DL models.

5. Discussion

COVID-19 has resulted in significant public health and safety concerns and has therefore become a worldwide issue [70]. Despite the paucity of PCR tests and their high cost [6], it was beneficial to make access to healthcare staff an artificial intelligence-based approach for rapidly and correctly predicting COVID-19. In this paper, we proposed an automated health monitoring system for the early diagnosis of COVID-19 using chest images that is less expensive, more accessible to rural populations, and has an easily disinfected, cleaned, and maintained acquisition apparatus. The SEL-COVIDNET model employs deep learning through nine pre-trained CNNs derived from the ImageNet database. Each network will predict a class based on the input image's classification. Our approach has the benefit of assigning a score to each class prediction.

Furthermore, it was conducted on balanced and balanced datasets. Through a thorough examination, the tuned InceptionResNetV2, MobileNetV3Large, and DenseNet121 models preserved the highest overall accuracy among other DL models. In that, the tuned InceptionResNetV2 achieved better performance for 3-class classification (COVID-19 vs. No-finding vs. Pneumonia) on dataset 1 with an overall test accuracy of 96.4%, an F1-score of 96.8%, a Sen of 96.6%, a Spc of 97.8%, a Ppv of 97%, and an MCC of 94.6%. Moreover, for the binary-class classification (COVID-19 vs. No-finding) on the same dataset, they had an accuracy score of 99.3%, an F1-score of 98.7%, a Sen of 97.4%, a Ppv of 99%.

The SEL-COVIDNET model with tuned DenseNet121 outperformed for 3-class classification on dataset 2 with an overall test accuracy of 98.52%, an F1-score of 98.6%, a Sen of 98.5%, a Spc of 98.9%, a Ppv

of 98.7%, and an MCC of 97.6%. And for the 2-class classification, we achieved an accuracy score of 99.8%, an F1-score of 99.7%, a Sen of 99.9%, and a Ppv of 99.6%.

Further, the tuned MobileNetV3Large model outperformed other DL models for 3-class classification on dataset 3 (balanced data) with an overall test accuracy of 96.25%, an F1-score of 96.2%, a Sen of 96.3%, a Spc of 98.1%, a Ppv of 96.3%, and an MCC of 94.4%. And for the 2-class classification, they attained an accuracy score of 99.35%, an F1-score of 99.4%, a Sen of 99.4%, and a Ppv of 99.4%. Prateek et al. [35] attained an overall test accuracy of 97.70%. In [30], the authors introduced the CNN approach, in which they implemented the experiment on binary-class and multi-class classifications and attained 98.08% and 87.02% accuracy for binary and multiclassification, respectively. Montalbo et al. [64] proposed a model based on truncated DenseNet and achieved an accuracy of 97.7% for 3-class classification. In [66], the researcher proposed a truncation method based on deep CNNs and achieved promising results, with 97.4% accuracy in 3-class classification.

For dataset 4 (CT-scan), the tuned MobileNetV3Large and MobileNetV2 models outperformed other DL models in the binary-class classification (COVID-19 vs. No-finding) with an overall test accuracy of 98.79%, an F1-score of 98.8%, a Sen of 98.8%, a Spc of 98.8%, a Ppv of 98.8%, and an MCC of 97.6%. Wang et al. [7] proposed a DL model for screening COVID-19 based on CT-Scan images and achieved an accuracy of 89.5%. In [67], researchers described a technique for classifying 2-class CT-Scan images based on deep feature concatenation. Their model attained an accuracy of 99.3%. However, Table 10 compares the proposed SEL-COVIDNET model to state-of-the-art (SOTA) methods from a broader perspective. The suggested SEL-COVIDNET model achieved a remarkable 98.52% accuracy. However, there is no direct comparison since each model has been trained on various classes and different datasets of examples of either X-ray or CT scan diagnosis. Thus, despite having a more challenging task, the SEL-COVIDNET architecture with the tuned model approach may be more effective and valuable in most cases than the previous research provided.

6. Conclusions

This study aimed to develop an intelligent method for early COVID-19 identification utilizing chest imaging. Due to the limited availability of PCR and CT testing in some developing nations, we have proposed a DL-based technique for early detection of COVID-19 using chest X-ray/CT images in this work. To do this, we employed transfer learning models for two-class classification (COVID-19 vs. No-finding) and three-class classification (COVID-19 vs. No-finding vs. Pneumonia), utilizing the transfer learning idea. We have fine-tuned nine pre-trained architectures, including DenseNet121, VGG19, and InceptionV3, InceptionResNetV2, ResNet50, ResNet101, MobileNetV2, MobileNetV3Small, and MobileNetV3Large. We use the tweaked nine models to create a stacking model that outperforms all other models. On the basis of the findings and analyses from the performed research, this study concludes that the suggested SEL-COVIDNET model can achieve superior results in diagnosing COVID-19 from chest image modalities. The presented model outperformed all other SOTA approaches.

In future works, we intend to test our approach in more medical areas, such as dementia and Alzheimer's disease, and breast cancer. Additionally, we plan to utilize this model to identify COVID-19 infections produced by genetically mutated viruses. We are also going to incorporate salience maps in order to increase the interpretability of the model, which is vital not only for clinical treatment but also for research. We intend to train the model on an intensified dataset comprised of different X-ray images. As a result, the model's accuracy and generalizability could be improved.

Declaration of competing interest

The authors declare that they have no known competing financial interests or personal relationships that could have appeared to influence the work reported in this paper.

Acknowledgment

The authors deeply acknowledge the Researchers supporting program (TUMA-Project-2021-27) Almaarefa University, Riyadh, Saudi Arabia for supporting steps of this work.

Funding

This research was supported by the Researchers Supporting Program (TUMA-Project-2021-27) Almaarefa University, Riyadh, Saudi Arabia.

Appendix

See Table 11, Figs. 10–13.

References

[1] WorldOmeter. COVID live - Coronavirus statistics - Worldometer. 2022, https://www.worldometers.info/coronavirus/. [Accessed 12 August 2022].
[2] Coronavirus Disease 2019 (COVID-19) | CDC. 2022, https://www.cdc.gov/coronavirus/2019-ncov/index.html. [Accessed 24 April 2022].
[3] COVID-19 quarantine and isolation | CDC. 2022, https://www.cdc.gov/coronavirus/2019-ncov/your-health/quarantine-isolation.html. [Accessed 24 April 2022].
[4] What you should know about Coronavirus disease 2019 (COVID-19)-ENT health. 2022, https://www.enthealth.org/be_ent_smart/what-you-should-know-about-coronavirus-disease-2019-covid-19/. [Accessed 24 April 2022].
[5] Shen M, Zhou Y, Ye J, Al-Maskri AAA, Kang Y, Zeng S, et al. Recent advances and perspectives of nucleic acid detection for coronavirus. J Pharm Anal 2020;10(2):97–101.
[6] Tahamtan A, Ardebili A. Real-time RT-PCR in COVID-19 detection: Issues affecting the results. Exp Rev Mol Diagn 2020;20(5):453–4.
[7] Wang S, Kang B, Ma J, Zeng X, Xiao M, Guo J, et al. A deep learning algorithm using CT images to screen for corona virus disease (COVID-19). European Radiology 2021;31(8):6096–104.
[8] Zheng C, Deng X, Fu Q, Zhou Q, Feng J, Ma H, et al. Deep learning-based detection for COVID-19 from chest CT using weak label. 2020, MedRxiv, Cold Spring Harbor Laboratory Press.
[9] Li L, Qin L, Xu Z, Yin Y, Wang X, Kong B, et al. Artificial intelligence distinguishes COVID-19 from community acquired pneumonia on chest CT. Radiology 2020.
[10] Song Y, Zheng S, Li L, Zhang X, Zhang X, Huang Z, et al. Deep learning enables accurate diagnosis of novel coronavirus (COVID-19) with CT images. IEEE/ACM Trans Comput Biol Bioinform 2021;18(6):2775–80.
[11] Wang L, Lin ZQ, Wong A. COVID-Net: A tailored deep convolutional neural network design for detection of COVID-19 cases from chest X-ray images. Sci Rep 2020;10(1):1–12.
[12] Shi F, Xia L, Shan F, Song B, Wu D, Wei Y, et al. Large-scale screening to distinguish between COVID-19 and community-acquired pneumonia using infection size-aware classification. Phys Med Biol 2021;66(6):065031.
[13] Li L, Qin L, Xu Z, Yin Y, Wang X, Kong B, et al. Using artificial intelligence to detect COVID-19 and community-acquired pneumonia based on pulmonary CT: Evaluation of the diagnostic accuracy. Radiology 2020;296(2):E65–71.
[14] Xu X, Jiang X, Ma C, Du P, Li X, Lv S, et al. A deep learning system to screen novel coronavirus disease 2019 pneumonia. Engineering 2020;6(10):1122–9.
[15] of North America RS. CT provides best diagnosis for COVID-19 – ScienceDaily. 2020, https://www.sciencedaily.com/releases/2020/02/200226151951.htm.
[16] Fang Y, Zhang H, Xie J, Lin M, Ying L, Pang P, et al. Sensitivity of chest CT for COVID-19: Comparison to RT-PCR. Radiology 2020;296(2):E115–7.
[17] A. Alsanabani A, A. Ahmed M, M. Al Smadi A. Vehicle counting using detecting-tracking combinations: A comparative analysis. In: 2020 the 4th international conference on video and image processing. 2020, p. 48–54. http://dx.doi.org/10.1145/3447450.3447458.
[18] Abugabah A, Mehmood A, Almotairi S, Smadi AA. Health care intelligent system: A neural network based method for early diagnosis of Alzheimer's disease using MRI images. Expert Syst 2022;e13003.
[19] Rostami M, Oussalah M. A novel explainable COVID-19 diagnosis method by integration of feature selection with random forest. Inform Med Unlocked 2022;30:100941.

[20] Hasan MK, Alam MA, Dahal L, Roy S, Wahid SR, Elahi MTE, et al. Challenges of deep learning methods for COVID-19 detection using public datasets. Inform Med Unlocked 2022;30:100945.

[21] Jahmunah V, Sudarshan VK, Oh SL, Gururajan R, Gururajan R, Zhou X, et al. Future IoT tools for COVID-19 contact tracing and prediction: A review of the state-of-the-science. Int J Imaging Syst Technol 2021;31(2):455–71.

[22] Narin A, Kaya C, Pamuk Z. Automatic detection of coronavirus disease (COVID-19) using X-ray images and deep convolutional neural networks. Pattern Anal Appl 2021;24(3):1207–20.

[23] Faust O, Hagiwara Y, Hong TJ, Lih OS, Acharya UR. Deep learning for healthcare applications based on physiological signals: A review. Comput Methods Programs Biomed 2018;161:1–13.

[24] Painuli D, Mishra D, Bhardwaj S, Aggarwal M. Forecast and prediction of COVID-19 using machine learning. In: Data science for COVID-19. Elsevier; 2021, p. 381–97.

[25] Moulaei K, Shanbehzadeh M, Mohammadi-Taghiabad Z, Kazemi-Arpanahi H. Comparing machine learning algorithms for predicting COVID-19 mortality. BMC Med Inform Decis Mak 2022;22(1):1–12.

[26] Pathak Y, Shukla PK, Tiwari A, Stalin S, Singh S. Deep transfer learning based classification model for COVID-19 disease. Irbm 2020.

[27] Rhanoui M, Ghouzali S. Hybrid machine and deep transfer learning based classification models for COVID-19 and pneumonia diagnosis using X-ray images. In: Advances in information, communication and cybersecurity: proceedings of ICI2C'21, vol. 357. Springer Nature; 2022, p. 403.

[28] Das D, Santosh K, Pal U. Truncated inception net: COVID-19 outbreak screening using chest X-rays. Phys Eng Sci Med 2020;43(3):915–25.

[29] Ozturk T, Talo M, Yildirim EA, Baloglu UB, Yildirim O, Acharya UR. Automated detection of COVID-19 cases using deep neural networks with X-ray images. Comput Biol Med 2020;121:103792.

[30] Khan AI, Shah JL, Bhat MM. CoroNet: A deep neural network for detection and diagnosis of COVID-19 from chest X-ray images. Comput Methods Programs Biomed 2020;196:105581.

[31] Apostolopoulos ID, Aznaouridis SI, Tzani MA. Extracting possibly representative COVID-19 biomarkers from X-ray images with deep learning approach and image data related to pulmonary diseases. J.Med Biol Eng 2020;40(3):462–9.

[32] Ucar F, Korkmaz D. COVIDiagnosis-Net: Deep Bayes-SqueezeNet based diagnosis of the coronavirus disease 2019 (COVID-19) from X-ray images. Med Hypotheses 2020;140:109761.

[33] Loey M, Smarandache F, M. Khalifa NE. Within the lack of chest COVID-19 X-ray dataset: A novel detection model based on GAN and deep transfer learning. Symmetry 2020;12(4):651.

[34] Luz E, Silva P, Silva R, Silva L, Guimarães J, Miozzo G, et al. Towards an effective and efficient deep learning model for COVID-19 patterns detection in X-ray images. Res Biomed Eng 2021;1–14.

[35] Chhikara P, Gupta P, Singh P, Bhatia T. A deep transfer learning based model for automatic detection of COVID-19 from chest X-rays. Turk J Electr Eng Comput Sci 2021;29(SI-1):2663–79.

[36] Apostolopoulos ID, Mpesiana TA. COVID-19: Automatic detection from X-ray images utilizing transfer learning with convolutional neural networks. Phys Eng Sci Med 2020;43(2):635–40.

[37] Hemdan EE-D, Shouman MA, Karar ME. COVIDx-Net: A framework of deep learning classifiers to diagnose COVID-19 in X-ray images. 2020, arXiv preprint arXiv:2003.11055.

[38] Mehmood A, Abugabah A, Smadi AA, Alkhawaldeh R. An intelligent information system and application for the diagnosis and analysis of COVID-19. In: International conference on intelligent computing & optimization. Springer; 2021, p. 391–6.

[39] Abugabah A, Mehmood A, Al Zubi AA, Sanzogni L. Smart COVID-3D-SCNN: A novel method to classify X-ray images of COVID-19. Comput Syst Sci Eng 2022;41(3):997.

[40] Maia M, Pimentel JS, Pereira IS, Gondim J, Barreto ME, Ara A. Convolutional support vector models: Prediction of coronavirus disease using chest X-rays. Information 2020;11(12):548.

[41] Ibrahim AU, Ozsoz M, Serte S, Al-Turjman F, Yakoi PS. Pneumonia classification using deep learning from chest X-ray images during COVID-19. Cogn Comput 2021;1–13.

[42] Sethy PK, Behera SK, Ratha PK, Biswas P. Detection of coronavirus disease (COVID-19) based on deep features and support vector machine. Int J Math Eng Manag Sci 2020;5(4).

[43] Toraman S, Alakus TB, Turkoglu I. Convolutional capsnet: A novel artificial neural network approach to detect COVID-19 disease from X-ray images using capsule networks. Chaos Solitons Fractals 2020;140:110122.

[44] Zhang J, Xie Y, Pang G, Liao Z, Verjans J, Li W, et al. Viral pneumonia screening on chest X-rays using confidence-aware anomaly detection. IEEE Trans Med Imaging 2020;40(3):879–90.

[45] Ghoshal B, Tucker A. Estimating uncertainty and interpretability in deep learning for coronavirus (COVID-19) detection. 2020, arXiv preprint arXiv:2003.10769.

[46] Panwar H, Gupta P, Siddiqui MK, Morales-Menendez R, Singh V. Application of deep learning for fast detection of COVID-19 in X-Rays using ncovnet. Chaos Solitons Fractals 2020;138:109944.

[47] Rahman T, Khandakar A, Qiblawey Y, Tahir A, Kiranyaz S, Kashem SBA, et al. Exploring the effect of image enhancement techniques on COVID-19 detection using chest X-ray images. Comput Biol Med 2021;132:104319.

[48] Talo M. X-Ray DataSet-1. 2020, URL https://github.com/muhammedtalo/covid-19/tree/master/X-Ray%20Image%20DataSet.

[49] Chowdhury MEH, Rahman T, Khandakar A, Mazhar R, Kadir MA, Mahbub ZB, et al. Can AI help in screening viral and COVID-19 Pneumonia? IEEE Access 2020;8:132665–76. http://dx.doi.org/10.1109/ACCESS.2020.3010287.

[50] Patel P. X-Ray-dataset-2. 2020, URL https://www.kaggle.com/prashant268/chest-xray-covid19-pneumonia.

[51] Asraf A. Balanced-X-Ray-dataset-3. 2020, URL https://www.kaggle.com/amanullahasraf/covid19-pneumonia-normal-chest-xray-pa-dataset.

[52] Eduardo P. CT-scan-dataset. 2020, URL https://www.kaggle.com/plameneduardo/sarscov2-ctscan-dataset.

[53] Simonyan K, Zisserman A. Very deep convolutional networks for large-scale image recognition. 2014, arXiv preprint arXiv:1409.1556.

[54] Szegedy C, Vanhoucke V, Ioffe S, Shlens J, Wojna Z. Rethinking the inception architecture for computer vision. In: Proceedings of the IEEE conference on computer vision and pattern recognition. 2016, p. 2818–26.

[55] Szegedy C, Liu W, Jia Y, Sermanet P, Reed S, Anguelov D, et al. Going deeper with convolutions. In: Proceedings of the IEEE conference on computer vision and pattern recognition. 2015.

[56] Szegedy C, Ioffe S, Vanhoucke V, Alemi AA. Inception-v4, inception-ResNet and the impact of residual connections on learning. In: Proceedings of the thirty-first AAAI conference on artificial intelligence. AAAI Press; 2017, p. 4278–84.

[57] He K, Zhang X, Ren S, Sun J. Deep residual learning for image recognition. 2015, http://dx.doi.org/10.48550/ARXIV.1512.03385, arXiv.

[58] Sandler M, Howard A, Zhu M, Zhmoginov A, Chen L-C. MobileNetV2: Inverted residuals and linear bottlenecks. 2018, http://dx.doi.org/10.48550/ARXIV.1801.04381, arXiv.

[59] Howard A, Sandler M, Chen B, Wang W, Chen L, Tan M, et al. Searching for MobileNetV3. In: 2019 IEEE/CVF international conference on computer vision. IEEE Computer Society; 2019, p. 1314–24. http://dx.doi.org/10.1109/ICCV.2019.00140.

[60] Huang G, Liu Z, Van Der Maaten L, Weinberger KQ. Densely connected convolutional networks. In: Proceedings of the IEEE conference on computer vision and pattern recognition. 2017, p. 4700–8.

[61] Al-Falluji RA, Katheeth ZD, Alathari B. Automatic detection of COVID-19 using chest X-ray images and modified ResNet18-based convolution neural networks. Comput Mater Continua 2021;1301–13.

[62] Singh KK, Siddhartha M, Singh A. Diagnosis of coronavirus disease (COVID-19) from chest X-ray images using modified XceptionNet. Romanian J Inf Sci Technol 2020;23(657):91–115.

[63] Abbas A, Abdelsamea MM, Gaber MM. Classification of COVID-19 in chest X-ray images using DeTraC deep convolutional neural network. Appl Intell 2021;51(2):854–64.

[64] Montalbo FJP. Diagnosing COVID-19 chest X-rays with a lightweight truncated DenseNet with partial layer freezing and feature fusion. Biomed Signal Process Control 2021;68:102583.

[65] Qjidaa M, Ben-Fares A, Amakdouf H, El Mallahi M, Alami B-e, Maaroufi M, et al. Recognizing COVID-19 from chest X-ray images for people in rural and remote areas based on deep transfer learning model. Multimedia Tools Appl 2022;1–21.

[66] Montalbo FJ. Truncating fined-tuned vision-based models to lightweight deployable diagnostic tools for SARS-CoV-2 infected chest X-rays and CT-scans. Multimedia Tools Appl 2022;1–29.

[67] Saad W, Shalaby WA, Shokair M, El-Samie FA, Dessouky M, Abdellatef E. COVID-19 classification using deep feature concatenation technique. J Ambient Intell Humaniz Comput 2022;13(4):2025–43.

[68] Lin M, Chen Q, Yan S. Network in network. 2013, arXiv preprint arXiv:1312.4400.

[69] Gabruseva T, Poplavskiy D, Kalinin A. Deep learning for automatic pneumonia detection. In: 2020 IEEE/CVF conference on computer vision and pattern recognition workshops. IEEE Computer Society; 2020, p. 1436–43. http://dx.doi.org/10.1109/CVPRW50498.2020.00183.

[70] Wang C, Horby PW, Hayden FG, Gao GF. A novel coronavirus outbreak of global health concern. Lancet 2020;395(10223):470–3.